

Long spin coherence length and bulk-like spin-orbit torque in ferrimagnetic multilayers

Jiawei Yu¹, Do Bang^{2†}, Rahul Mishra^{1†}, Rajagopalan Ramaswamy¹, Jung Hyun Oh³, Hyeon-Jong Park⁴, Yunboo Jeong⁵, Pham Van Thach², Dong-Kyu Lee³, Gyungchoon Go³, Seo-Won Lee³, Yi Wang¹, Shuyuan Shi¹, Xuepeng Qiu⁶, Hiroyuki Awano², Kyung-Jin Lee^{3,4,5*}, and Hyunsoo Yang^{1*}

¹ Department of Electrical and Computer Engineering, National University of Singapore, 117576, Singapore

² Toyota Technological Institute, Tempaku, Nagoya 468-8511, Japan

³ Department of Materials Science and Engineering, Korea University, Seoul 02841, Korea

⁴ KU-KIST Graduate School of Converging Science and Technology, Korea University, Seoul 02841, Korea

⁵ Department of Semiconductor Systems Engineering, Korea University, Seoul 02841, Korea

⁶ Shanghai Key Laboratory of Special Artificial Macrostructure Materials and Technology and School of Physics Science and Engineering, Tongji University, Shanghai 200092, China

[†]These authors contributed equally to this work.

*e-mail: eleyang@nus.edu.sg, kj_lee@korea.ac.kr

Spintronics is a multidisciplinary field whose central theme is the active manipulation of spin degrees of freedom in solid-state systems. Ferromagnetic spintronics has been a main focus as it offers non-volatile memory and logic applications through current-induced spin-transfer torques¹⁻⁴. Enabling wider applications of such magnetic devices requires a lower switching current for a smaller cell while keeping the thermal stability of magnetic cells for non-volatility. As the cell size reduces, however, it becomes extremely difficult to meet this requirement with ferromagnets because spin-transfer torque for ferromagnets is a surface torque due to rapid spin dephasing^{5,6}, leading to the 1/ferromagnet-thickness dependence of the spin-torque efficiency⁷. Requirement of a larger switching current for a thicker and thus

more thermally stable ferromagnetic cell is the fundamental obstacle for high-density non-volatile applications with ferromagnets. Theories predicted that antiferromagnets have a long spin coherence length due to the staggered spin order on an atomic scale^{8,9}, thereby resolving the above fundamental limitation. Despite several spin-torque experiments on antiferromagnets¹⁰⁻¹² and ferrimagnetic alloys¹³⁻¹⁶, this prediction has remained unexplored. Here we report a long spin coherence length and associated bulk-like-torque characteristic in an antiferromagnetically coupled ferrimagnetic multilayer. We find that a transverse spin current can pass through > 10 nm-thick ferrimagnetic Co/Tb multilayers whereas it is entirely absorbed by 1 nm-thick ferromagnetic Co/Ni multilayer. We also find that the switching efficiency of Co/Tb multilayers partially reflects a bulk-like-torque characteristic as it increases with the ferrimagnet-thickness up to 8 nm and then decreases, in clear contrast to 1/thickness-dependence of Co/Ni multilayers. Our results on antiferromagnetically coupled systems will invigorate researches towards energy-efficient spintronic technologies.

The spin-transfer torque (STT) acting on ferromagnets (FMs) is a surface torque, based on the averaging effect of STT^{5,6}. We note that the same averaging effect occurs regardless of the spin-current source, and the spin-orbit torque (SOT)^{17,18}, which we use in our experiment, is also a surface torque for FMs (Extended Data Fig. 1 and Methods). When a transverse spin current with a spin orientation non-collinear with the magnetization is injected into a FM, the electron spin precesses rapidly in real space because the wave vectors of the majority (\uparrow) and minority (\downarrow) spins at the Fermi surface are different (i.e., $k_F^\uparrow \neq k_F^\downarrow$). The precession wavelengths are different for different incident angles of electrons (i.e., the direction of wave vector \mathbf{k}), leading to rapid spin dephasing when summing over all current-carrying \mathbf{k} -states. As a result, the \mathbf{k} -integrated transverse spin current decays to zero within a distance from the FM surface, called the ferromagnetic

coherence length (spin coherence length, more generally), $\lambda_c = \pi/|k_F^\uparrow - k_F^\downarrow|$.¹⁹ As $|k_F^\uparrow - k_F^\downarrow|$ becomes larger for larger exchange splitting, λ_c is only a few angstroms in strong FMs (e.g. cobalt or iron) for which the STT is almost a surface torque.

Theories predicted that the spin coherence length is very long in antiferromagnets (AFMs) because of the staggered spin order on an atomic scale^{8,9}. We use the term of “bulk-like-torque” to describe the characteristic of spin-torque for AFMs, i.e., spin-current absorption on a larger thickness, in contrast to the surface-torque of FMs. A semi-classical explanation of bulk-like-torque is that for conduction electron spins, the moments with alternating orientation on an atomic scale are seen as the exchange interactions with alternating signs. As a result, an ideal AFM has zero net effective exchange interaction when averaged over two sub-lattices and thus has an infinitely long λ_c , yielding the bulk-like-torque characteristic. Several experiments have investigated on STT/SOT effects in systems including AFMs¹⁰⁻¹² and more recently on ferrimagnetic alloys¹³⁻¹⁶, but not on the long spin coherence length and associated bulk-like-torque characteristic.

We qualitatively illustrate the spin coherence length in FMs and FIMs (or AFMs) based on the spin precession around the local exchange field. Neglecting the spin relaxation, dynamics of non-equilibrium spin density \mathbf{s} is described by $\partial\mathbf{s}/\partial t = -\gamma \mathbf{s} \times \mathbf{H}_{ex}$, where γ is the gyromagnetic ratio, \mathbf{H}_{ex} is the effective exchange field that is aligned along the local magnetic moment \mathbf{m} . Assuming $\mathbf{s} = (\sin\theta, \cos\theta, 0)$ and $\mathbf{H}_{ex} = H\hat{\mathbf{z}}$, this equation of motion transforms to $\partial\theta/\partial t = \delta\theta/\delta t = -\gamma H$, where the sign of spin precession angle $\delta\theta$ follows the sign of H and thus the sign of \mathbf{m} (Fig. 1a and b). In a FM, an electron spin propagating along the x -direction continuously precesses in the same sense because of the homogeneous exchange field (Fig. 1c). On the other hand, in a FIM, an electron spin precesses counter-clockwise on a lattice corresponding to a positive exchange field,

whereas it precesses clockwise on the next lattice corresponding to a negative exchange field. As a result, the period (or wavelength) of spin precession in FIMs is longer than that in FMs, resulting in much less spin dephasing.

In order to verify the theoretical prediction of long spin coherence length, we perform experiments with a ferrimagnet (FIM), i.e., Co/Tb multilayers where both Co and Tb layers are atomically thin and their moments are coupled antiferromagnetically. We choose a FIM, instead of an AFM, for following two reasons. One is that Co/Tb multilayers can show a longer λ_c than a FM because of the antiferromagnetic alignment of Co and Tb moments (Extended Data Fig. 1 and Methods), thereby exhibiting a feature of the bulk-like-torque characteristic. As explained above, the STT efficiency of a FM is inversely proportional to the FM-thickness whereas that of an ideal AFM is independent of the AFM-thickness. As λ_c of FIM is located between those of FM and AFM, it is expected that the STT efficiency of a FIM first increases and then decreases with the FIM-thickness. The other reason to choose FIMs is that various measurement methods established for FMs are applicable to FIMs because of nonzero net moment^{13,20}. However, the choice of FIM also results in a difficulty. FIMs commonly show a thickness-dependent variation of magnetic properties²¹, as also observed in Co/Tb multilayers (Extended Data Fig. 4 and Methods), which makes a quantitative analysis of spin transport difficult. Even with this difficulty, our thickness-dependent SOT measurements combined with spin pumping measurements support a long spin coherence length and associated bulk-like-torque characteristic in ferrimagnetic Co/Tb multilayers, as we show below.

We fabricate perpendicularly magnetized ferromagnetic [Co/Ni]_N and ferrimagnetic [Co/Tb]_N multilayers (Fig. 2a, b; see Methods for details), where the total thickness varies with changing the repetition number *N*. Both Co/Ni and Co/Tb multilayers have an additional Pt layer, and an in-

plane current generates SOTs. We use the harmonic Hall voltage measurements to quantify the strength of SOT effective fields^{22,23}. The longitudinal and transverse measurement schematics are illustrated in Fig. 2c and d, respectively. Representative results for the longitudinal (blue line) and transverse (red line) second harmonic voltages (V_{2f}) from Co/Ni ($N = 2$) and Co/Tb ($N = 5$) devices are shown in Fig. 2e and f, respectively. The anomalous Nernst effect is corrected in the V_{2f} data²². We observe a clear V_{2f} in the longitudinal configuration (H//I), which is mostly determined by the anti-damping SOT^{22,23}. The opposite V_{2f} signs in the H//I case for Co/Ni and Co/Tb multilayers indicate that the Pt layer is the source of spin currents, as it is placed on top of the Co/Tb multilayer, but under the Co/Ni multilayer. In order to rule out the contribution from pure bulk Co/Tb to SOT, we conduct a control experiment without and with the spin current source, Pt (Extended Data Fig. 5, 6 and Methods). We find that there is no noticeable current-induced SOT without the Pt layer, suggesting that the Co/Tb bulk itself cannot directly contribute to SOTs.

We extract the spin-orbit effective fields, H_L and H_T , by fitting V_{2f} ²³ where H_L and H_T correspond to the anti-damping (longitudinal) and field-like (transverse) components of SOTs, respectively. The planar Hall effect is considered for the fitting (Extended Data Fig. 8 and Methods). Devices with different N , corresponding to different thicknesses, t_{FM} or t_{FIM} , have been measured. Absolute SOT effective fields normalized by the current density in the Pt layer ($H_{L/T}/J$) are presented in Fig. 3a and b for the Co/Ni and Co/Tb systems, respectively. We find that both H_L and H_T of Co/Ni multilayers decrease as t_{FM} increases, consistent with the surface-torque characteristic expected for FMs. However, Co/Tb multilayers show an entirely different trend, in which both H_L and H_T increase up to t_{FIM} of 7.9 nm and then decrease for thicker samples.

We estimate the effective spin Hall angle $\theta_{eff} = H_L (2eM_S t_{FM/FIM} / \hbar J)$, where e is the electron charge and \hbar is the reduced Planck's constant, with considering thickness-dependent variation of

the saturation magnetization M_S and current density J in the Pt layer. The Co/Tb multilayer shows a significant M_S variation with the minimum at t_{FIM} of 6.6 nm (inset of Fig. 3d). We find that θ_{eff} of Co/Ni multilayer is nearly constant with t_{FIM} (Fig. 3c). Similar to the tendency of H_L/J , θ_{eff} of Co/Tb multilayer increases up to $t_{\text{FIM}} = 9.9$ nm and then decreases for a thicker sample (Fig. 3d). Besides the distinct thickness-dependence of θ_{eff} , another interesting observation is that the Co/Tb multilayer shows a larger θ_{eff} than Co/Ni multilayer (θ_{eff} of Co/Tb multilayer = 2.1 at t_{FIM} of 9.9 nm and the average θ_{eff} of Co/Ni multilayer = 0.2 ± 0.05). We note that a model calculation with considering a thickness-dependent variation of the sd exchange in FIMs shows qualitatively similar trends with the experimental ones (Extended Data Fig. 2 and Methods), even though the model is too simple to capture all the details of FIMs. Nevertheless, this qualitative agreement between model and experiment results indicates that the distinct behavior of θ_{eff} of Co/Tb multilayer would originate from a combined effect of long spin coherence length and thickness-dependent property variation.

As an independent test, we perform SOT switching experiments with applying an external field (H_{ext}) in the current direction ($\theta = 0^\circ$) for deterministic switching. The insets of Fig. 3e and f show the representative current-induced switching data obtained from Co/Ni ($N = 2$) and Co/Tb ($N = 5$) samples, respectively. As the switching is governed by domain nucleation and propagation in large samples (i.e., Hall bar width = 10 μm), we estimate the STT efficiency $\eta = H_p / J$, where H_p is the domain wall depinning field²⁴. Figure 3e and f show η as a function of t_{FM} and t_{FIM} , respectively. For Co/Ni multilayers, η decreases with t_{FM} , whereas for Co/Tb multilayers it increases and then decreases with t_{FIM} , following similar trends to SOT effective fields (Fig. 3a and b). We note that recently reported fast dynamics at the angular momentum compensation condition in FIMs²⁰ would affect the switching data, but not the harmonic Hall data.

As different approaches for the estimation of spin torque efficiency show qualitatively similar trends, it indicates that SOT for Co/Tb multilayers is not a surface torque. Moreover, the observed thickness-dependence of spin torque efficiency is qualitatively consistent with the model calculation (Extended Data Fig. 2 and Methods) for the bulk-like-torque characteristic in FIMs; it first increases and then decreases with the FIM-thickness. However, because of the thickness-dependent property variations in Co/Tb multilayers (inset of Fig. 3d and Methods), this result is not yet conclusive but it is still possible that another unknown mechanism is responsible for the distinct thickness-dependence observed in Co/Tb multilayers.

In order to resolve this ambiguity, we perform additional spin pumping experiments to estimate the spin coherence length λ_c . We measure a spin-pumping-induced inverse spin Hall voltage (V_{ISHE}) for substrate/Pt(10)/[FIM or FM]/Cu(2.4)/Co(20) structures (numbers in nanometers; FIM = [Co(0.32)/Tb(0.34)] $_N$ and FM = [Co(0.3)/Ni(0.6)] $_N$) as shown in Fig. 4a. In these structures, the Co/Ni and Co/Tb multilayers are perpendicularly magnetized, whereas the top thick Co layer has an in-plane magnetization. In the spin pumping setup (Fig. 4b; see Methods for details), the top Co layer generates a spin-pumping-induced spin current with an in-plane spin polarization (thus transverse to Co/Ni or Co/Tb magnetization direction), which passes through the Cu layer and enters the Co/Ni or Co/Tb layer. If λ_c of the Co/Tb multilayer is long, it is expected that a transverse spin current passes through the Co/Tb layer without much spin dephasing and reaches the bottom spin sink, Pt, and subsequently, V_{ISHE} is generated by the inverse spin Hall effect of Pt. On the other hand, V_{ISHE} is expected to be negligible for a thick Co/Ni multilayer because a transverse spin current is almost absorbed at the [Co/Ni]/Cu interface. Therefore, the measurement of V_{ISHE} versus FIM- or FM-thickness provides an estimate of λ_c .

We find that the experimental results are consistent with this expectation. In Fig. 4c, black symbols are the data from a reference Pt/Cu/Co sample, which shows the largest V_{ISHE} signal at an in-plane bias field H_b . For the Co/Ni-based structure, V_{ISHE} signal becomes negligible at a Co/Ni thickness of 0.9 nm (blue symbols). In contrast, V_{ISHE} signal for the Co/Tb-based structure is finite at a much thicker Co/Tb (red symbols, Co/Tb thickness = 5.3 nm as an example). V_{ISHE} signal disappears when excluding the top Co layer from the Co/Tb-based structure (green symbol), proving that the perpendicularly magnetized Co/Tb itself does not generate a V_{ISHE} signal. In Fig. 4d, spin pumping results are summarized for a wide thickness range of Co/Tb multilayer. It shows that V_{ISHE} signal is finite even at 13 nm-thick Co/Tb. This result evidences a long spin coherence length in ferrimagnetic Co/Tb multilayers.

The spin pumping and spin torque are connected through the Onsager reciprocity²⁵. Therefore, the long spin coherence length observed in spin pumping experiments suggests that the bulk-like-torque characteristic must be present in spin torque experiments at least partially. Given that the thickness-dependent change in the spin torque efficiency follows the trend expected for the bulk-like-torque characteristic (Fig. 3), the spin pumping experiments combined with the spin torque experiments allow us to conclude that the antiferromagnetically coupled FIMs show a long spin coherence length and associated bulk-like-torque characteristic. We note that this bulk-like-torque characteristic and equivalently long spin coherence length are also observed for FIM alloys (Extended Data Fig. 9 and Methods), which would relate to some ordering in FIM alloys^{26,27}. The results were supported by model calculation using a ferrimagnetic alloy (Extended Data Fig. 2 and Methods) in which an ordered alloy shows a longer spin coherence length than a random alloy. These salient features make antiferromagnetically coupled FIMs attractive for low-power non-volatile applications. We expect the bulk-like-torque principle is also applicable to domain wall or

skyrmion devices²⁸⁻³⁰ operated by SOTs. In this respect, our findings will motivate research activities to introduce FIMs as core elements in spintronics devices, which have been so far dominated by FMs. Therefore, our result provides an important step towards “ferrimagnetic spintronics”.

References

- 1 Slonczewski, J. C. Current-driven excitation of magnetic multilayers. *J. Magn. Magn. Mater.* **159**, L1-L7, (1996).
- 2 Berger, L. Emission of spin waves by a magnetic multilayer traversed by a current. *Phys. Rev. B* **54**, 9353-9358, (1996).
- 3 Tsoi, M. *et al.* Excitation of a Magnetic Multilayer by an Electric Current. *Phys. Rev. Lett.* **80**, 4281-4284, (1998).
- 4 Myers, E. B., Ralph, D. C., Katine, J. A., Louie, R. N. & Buhrman, R. A. Current-Induced Switching of Domains in Magnetic Multilayer Devices. *Science* **285**, 867-870, (1999).
- 5 Waintal, X., Myers, E. B., Brouwer, P. W. & Ralph, D. C. Role of spin-dependent interface scattering in generating current-induced torques in magnetic multilayers. *Phys. Rev. B* **62**, 12317-12327, (2000).
- 6 Stiles, M. D. & Zangwill, A. Anatomy of spin-transfer torque. *Phys. Rev. B* **66**, 014407, (2002).
- 7 Albert, F. J., Emley, N. C., Myers, E. B., Ralph, D. C. & Buhrman, R. A. Quantitative Study of Magnetization Reversal by Spin-Polarized Current in Magnetic Multilayer Nanopillars. *Phys. Rev. Lett.* **89**, 226802, (2002).
- 8 Núñez, A. S., Duine, R. A., Haney, P. & MacDonald, A. H. Theory of spin torques and giant magnetoresistance in antiferromagnetic metals. *Phys. Rev. B* **73**, 214426, (2006).
- 9 Haney, P. M. & MacDonald, A. H. Current-Induced Torques Due to Compensated Antiferromagnets. *Phys. Rev. Lett.* **100**, 196801, (2008).
- 10 Wei, Z. *et al.* Changing Exchange Bias in Spin Valves with an Electric Current. *Phys. Rev. Lett.* **98**, 116603, (2007).
- 11 Urazhdin, S. & Anthony, N. Effect of Polarized Current on the Magnetic State of an Antiferromagnet. *Phys. Rev. Lett.* **99**, 046602, (2007).
- 12 Wadley, P. *et al.* Electrical switching of an antiferromagnet. *Science*, **351**, 587(2016).
- 13 Mishra, R. *et al.* Anomalous Current-Induced Spin Torques in Ferrimagnets near Compensation. *Phys. Rev. Lett.* **118**, 167201, (2017).
- 14 Finley, J. & Liu, L. Spin-Orbit-Torque Efficiency in Compensated Ferrimagnetic Cobalt-Terbium Alloys. *Phys. Rev. Applied* **6**, 054001, (2016).
- 15 Roschewsky, N., Lambert, C.-H. & Salahuddin, S. Spin-orbit torque switching of ultralarge-thickness ferrimagnetic GdFeCo. *Phys. Rev. B* **96**, 064406, (2017).
- 16 Ueda, K., Mann, M., de Brouwer, P. W. P., Bono, D. & Beach, G. S. D. Temperature dependence of spin-orbit torques across the magnetic compensation point in a ferrimagnetic TbCo alloy film. *Phys. Rev. B* **96**, 064410, (2017).
- 17 Miron, I. M. *et al.* Perpendicular switching of a single ferromagnetic layer induced by in-plane current injection. *Nature* **476**, 189-193, (2011).
- 18 Liu, L. *et al.* Spin-Torque Switching with the Giant Spin Hall Effect of Tantalum. *Science* **336**, 555-558, (2012).
- 19 Kovalev, A. A., Bauer, G. E. W. & Brataas, A. Perpendicular spin valves with ultrathin ferromagnetic layers: Magnetoelectronic circuit investigation of finite-size effects. *Phys. Rev. B* **73**, 054407, (2006).
- 20 Kim, K.-J. *et al.* Fast domain wall motion in the vicinity of the angular momentum compensation temperature of ferrimagnets. *Nature Mater.* **16**, 1187-1192, (2017).

- 21 Hebler, B., Hassdenteufel, A., Reinhardt, P., Karl, H. & Albrecht, M. Ferrimagnetic Tb–
Fe Alloy Thin Films: Composition and Thickness Dependence of Magnetic Properties and
All-Optical Switching. *Frontiers in Materials* **3**, 8 (2016).
- 22 Garello, K. *et al.* Symmetry and magnitude of spin-orbit torques in ferromagnetic
heterostructures. *Nature Nanotechnol.* **8**, 587-593, (2013).
- 23 Kim, J. *et al.* Layer thickness dependence of the current-induced effective field vector in
Ta|CoFeB|MgO. *Nature Mater.* **12**, 240-245, (2013).
- 24 Lee, O. J. *et al.* Central role of domain wall depinning for perpendicular magnetization
switching driven by spin torque from the spin Hall effect. *Phys. Rev. B* **89**, 024418, (2014).
- 25 Brataas, A., Kent, A. D. & Ohno, H. Current-induced torques in magnetic materials. *Nature
Mater.* **11**, 372, (2012).
- 26 Graves, C. E. *et al.* Nanoscale spin reversal by non-local angular momentum transfer
following ultrafast laser excitation in ferrimagnetic GdFeCo. *Nature Mater.* **12**, 293,
(2013).
- 27 Chimata, R. *et al.* All-thermal switching of amorphous Gd-Fe alloys: Analysis of structural
properties and magnetization dynamics. *Phys. Rev. B* **92**, 094411, (2015).
- 28 Emori, S., Bauer, U., Ahn, S.-M., Martinez, E. & Beach, G. S. D. Current-driven dynamics
of chiral ferromagnetic domain walls. *Nature Mater.* **12**, 611-616, (2013).
- 29 Ryu, K.-S., Thomas, L., Yang, S.-H. & Parkin, S. Chiral spin torque at magnetic domain
walls. *Nature Nanotechnol.* **8**, 527-533, (2013).
- 30 Sampaio, J., Cros, V., Rohart, S., Thiaville, A. & Fert, A. Nucleation, stability and current-
induced motion of isolated magnetic skyrmions in nanostructures. *Nature Nanotechnol.* **8**,
839-844, (2013).
- 31 Qiu, X. *et al.* Angular and temperature dependence of current induced spin-orbit effective
fields in Ta/CoFeB/MgO nanowires. *Sci. Rep.* **4**, 4491, (2014).
- 32 Sinova, J., Valenzuela, S. O., Wunderlich, J., Back, C. H. & Jungwirth, T. Spin Hall effects.
Rev. Mod. Phys. **87**, 1213-1260, (2015).
- 33 Tanaka, T. *et al.* Intrinsic spin Hall effect and orbital Hall effect in 4d and 5d transition
metals. *Phys. Rev. B* **77**, 165117, (2008).
- 34 Negele, J. W. & Orland, H. Quantum many-particle systems. *Boulder, Co: Westview*,
(1988).
- 35 Datta, S. Nanoscale device modeling: the Green's function method. *Superlattice and
Microstructures* **28**, 4, (2000).
- 36 Freimuth, F., Blügel, S. & Mokrousov, Y. Spin-orbit torques in Co/Pt(111) and
Mn/W(001) magnetic bilayers from first principles. *Phys. Rev. B* **90**, 174423, (2014).
- 37 Jamali, M. *et al.* Spin-Orbit Torques in Co/Pd Multilayer Nanowires. *Phys. Rev. Lett.* **111**,
246602, (2013).
- 38 Huang, K.-F., Wang, D.-S., Lin, H.-H. & Lai, C.-H. Engineering spin-orbit torque in Co/Pt
multilayers with perpendicular magnetic anisotropy. *Appl. Phys. Lett.* **107**, 232407, (2015).
- 39 Emori, S. *et al.* Spin Hall torque magnetometry of Dzyaloshinskii domain walls. *Phys. Rev.
B* **90**, 184427, (2014).
- 40 Harris, V. G., Aylesworth, K. D., Das, B. N., Elam, W. T. & Koon, N. C. Structural origins
of magnetic anisotropy in sputtered amorphous Tb-Fe films. *Phys. Rev. Lett.* **69**, 1939-
1942, (1992).
- 41 Hufnagel, T. C., Brennan, S., Zschack, P. & Clemens, B. M. Structural anisotropy in
amorphous Fe-Tb thin films. *Phys. Rev. B* **53**, 12024-12030, (1996).

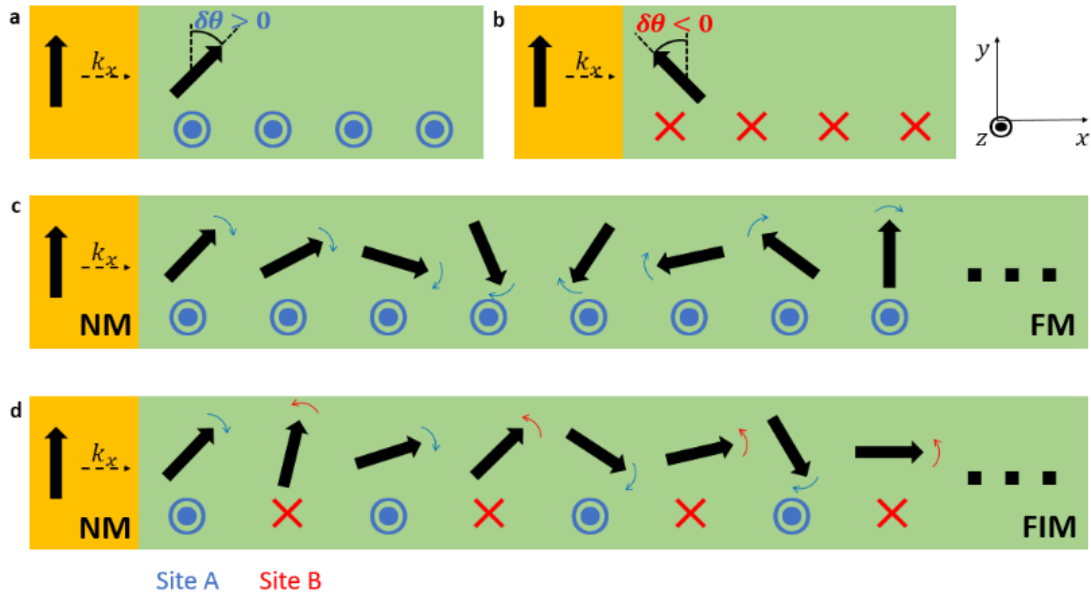


Figure 1 | Schematic illustrations of spin precession from the semi-classical viewpoint. a, b, Local spin precession angle $\delta\theta$ in a FM with up magnetic moment ($\mathbf{m} // +\hat{z}$) and down magnetic moment ($\mathbf{m} // -\hat{z}$), respectively. Blue dots (Fig. 1a) and red crosses (Fig. 1b) indicate the directions of magnetic moments. Precession of an electron spin in the FM layer (c) and in the FIM layer (d). Blue and red curved arrows indicate $\delta\theta > 0$ and $\delta\theta < 0$, respectively.

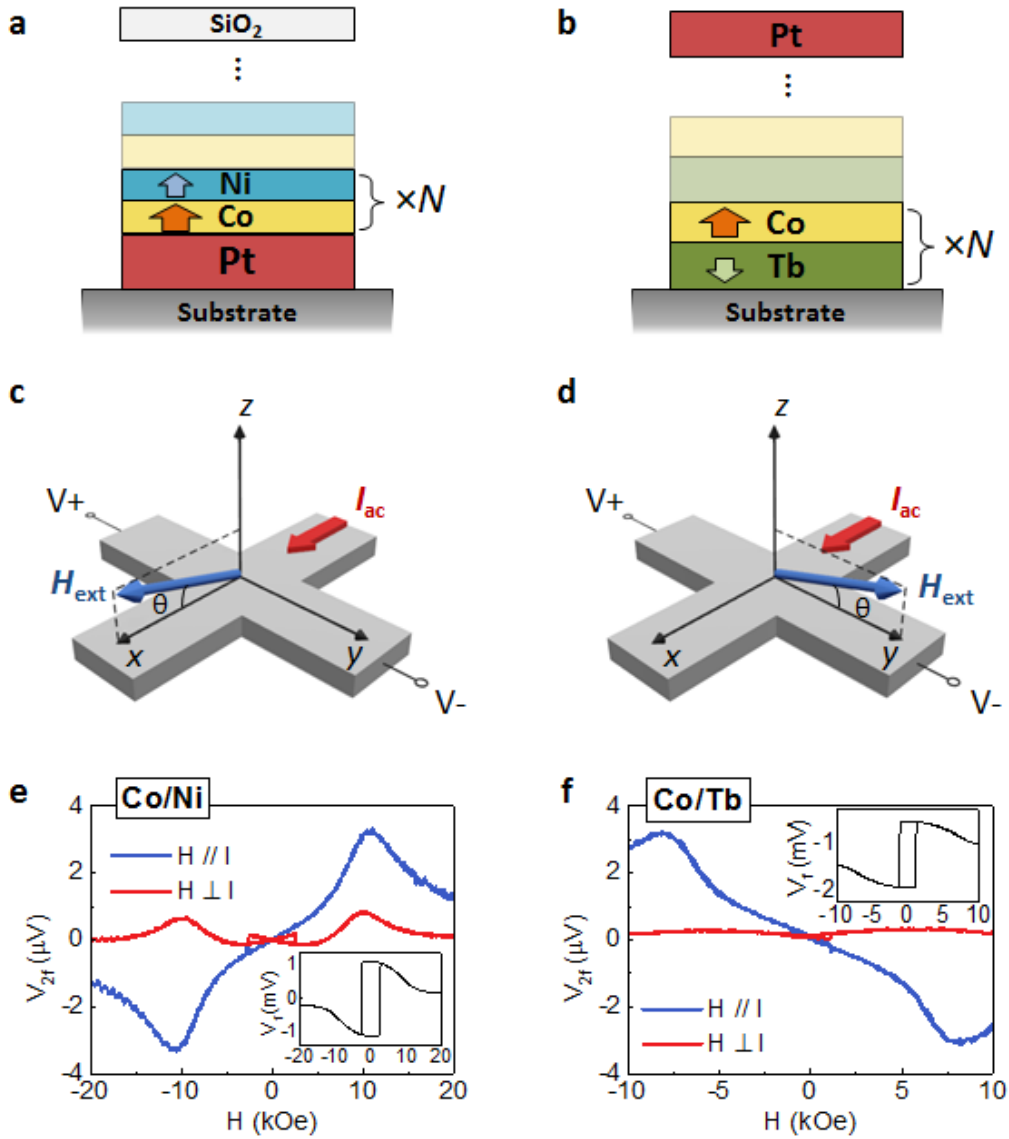


Figure 2 | Film stacks and SOT measurements. **a, b**, Illustrations of Co/Ni (**a**) and Co/Tb (**b**) multilayers. The magnetizations of Co, Ni and Tb sub-lattices are presented by the yellow, blue and green arrows, respectively. **c, d**, The measurement schematics for longitudinal (**c**) and transverse (**d**) SOT effective fields. **e, f**, Second harmonic voltages (V_{2f}) obtained from Co/Ni (**e**) and Co/Tb (**f**) multilayer devices, with the blue curves representing the longitudinal signals and red curves representing the transverse signals. The insets correspond to first harmonic voltages (V_{1f}).

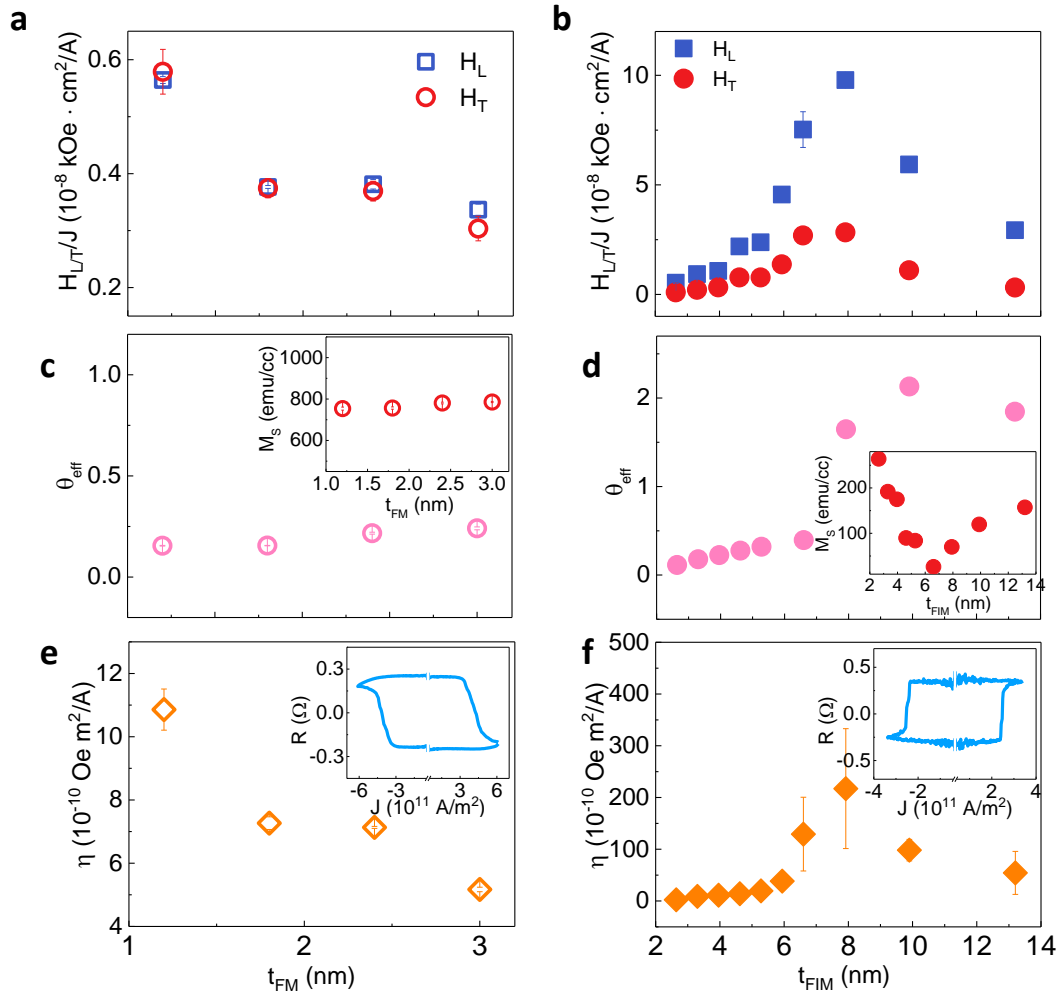


Figure 3 | SOT effective fields and switching efficiencies. **a, b**, Longitudinal (H_L) and transverse (H_T) SOT effective fields as a function of Co/Ni (**a**) or Co/Tb (**b**) thicknesses. **c, d**, Effective spin Hall angle (θ_{eff}) as a function of Co/Ni (**c**) or Co/Tb (**d**) thicknesses. Insets in **c** and **d** are the saturation magnetization (M_S) as a function of ferromagnet- or ferrimagnet-thickness. **e, f**, Switching efficiencies (η) as a function of Co/Ni (**e**) or Co/Tb (**f**) thicknesses. Insets in **e** and **f** are current-induced switching data, showing the Hall resistance (R_H) as a function of applied pulse current.

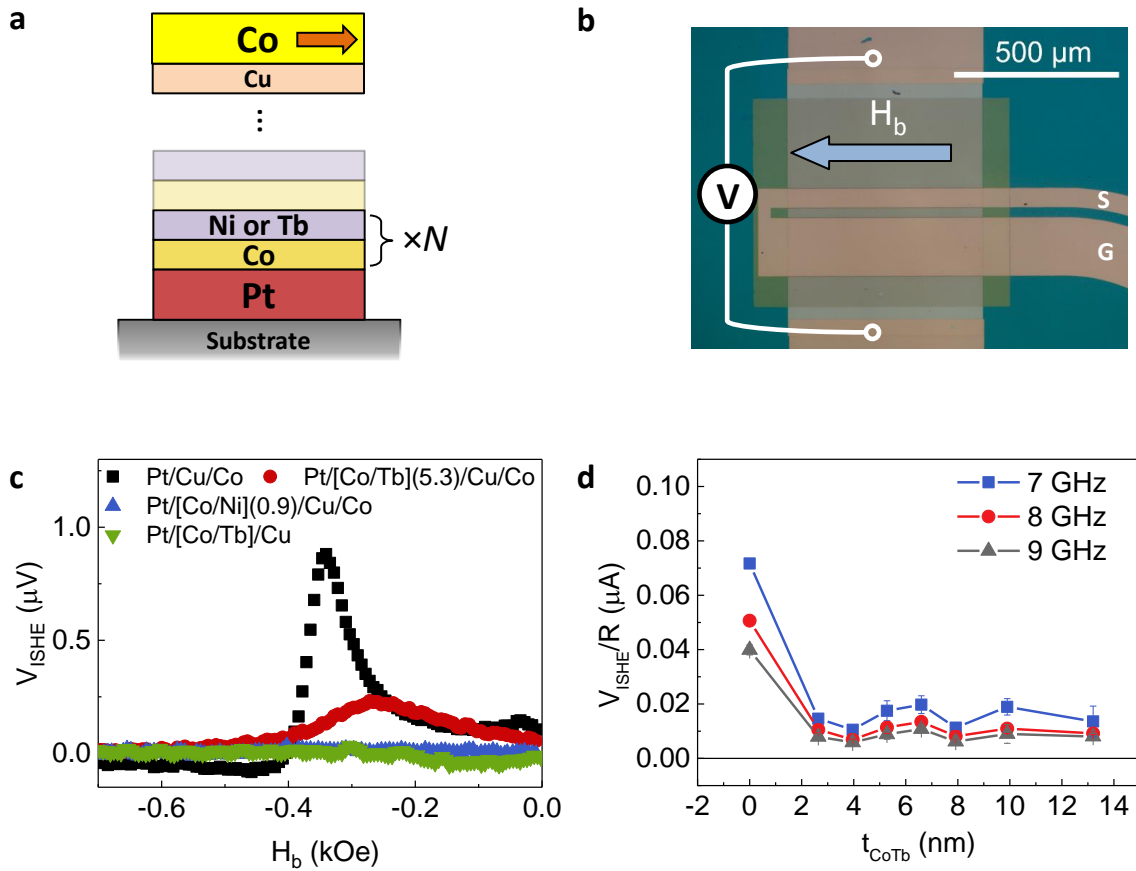


Figure 4 | Spin pumping measurements. **a**, Spin pumping sample structure. **b**, Schematic of spin pumping measurements. S and G indicates signal and ground connection for high frequency measurements. An in-plane field (H_b) along the waveguide direction is applied. **c**, Spin pumping signals in various structures. **d**, Inverse spin Hall signal as a function of [Co/Tb]-thickness in Pt/[Co/Tb]/Cu/Co structures at various frequencies.

Methods

Sample preparation

Substrate/[Tb (0.34 nm)/Co (0.32 nm)]_N/Pt (4 nm) and substrate/MgO (2 nm)/Pt (4 nm)/[Co (0.3 nm)/Ni (0.3 nm)]_N/SiO₂ (3 nm) multilayers are fabricated on thermally oxidized silicon substrates using rf and dc magnetron sputtering system with a base pressure of $\sim 10^{-9}$ Torr. N is the repetition number of Tb/Co or Co/Ni bilayer pairs, which is varied from 4 to 20 for Co/Tb systems and from 2 to 5 for Co/Ni systems. For Co/Tb multilayers, a 4 nm-thick Pt layer is deposited on top as a spin current source which also protects the multilayer from being oxidized. For Co/Ni multilayers, a bilayer of MgO (2 nm)/Pt (4 nm) is deposited on the bottom as a buffer and spin current source, and a SiO₂ (3 nm) layer is deposited as a capping layer to prevent possible oxidation of the FM layer. Subsequent photolithography and ion milling processes are performed to fabricate the films into Hall bar devices.

Second harmonic and spin pumping measurements

For the second harmonic measurements, an ac current I_{ac} with a frequency of 13.7 Hz and a magnitude of 5 mA is injected into the channel of the device³¹. An external magnetic field H_{ext} is applied along (orthogonal to) the current direction with a small out-of-plane tilting of $\theta = 4^\circ$ from the film plane in the longitudinal (transverse) configuration. The first and second harmonic Hall voltages are recorded simultaneously by using two lock-in amplifiers triggered at the same frequency by the current source.

In the spin pumping measurements, a microwave at 7 to 9 GHz is applied to the asymmetric coplanar stripline waveguide by a signal generator. An in-plane field (H_b) along the waveguide direction is swept around the resonance field (H_0) given by the Kittel formula

$$f = \frac{\gamma}{2\pi} \sqrt{H_0(H_0 + 4\pi M_S)},$$
 where γ is the gyromagnetic ratio and M_S is the saturation

magnetization. The voltage (V) is recorded by a lock-in amplifier. V includes the asymmetric component (V_{asym}) from the anomalous Hall effect (AHE) and the anisotropic magnetoresistance, as well as the symmetric components (V_{sym}) from the spin pumping induced inverse spin Hall voltage (V_{ISHE}). Thus the measured voltage is fitted by a sum of symmetric and asymmetric

Lorentzian function $V = V_{\text{sym}} \frac{\Gamma^2}{\Gamma^2 + (H - H_0)^2} + V_{\text{asym}} \frac{\Gamma(H - H_0)}{\Gamma^2 + (H - H_0)^2}$, from which V_{ISHE} is extracted

as V_{sym} .